A Frequency-Fixed SOGI Based PLL for Single-Phase Grid-Connected Converters

Furong Xiao[1], Lei Dong[1], Li Li[2], Xiaozhong Liao[1]

[1] School of Automation, Beijing Institute of Technology, Beijing, China

[2] Faculty of Engineering and Information Technology, University of Technology, Sydney, Australia

Corresponding Author: Lei Dong, Associate Professor, School of Automation in Beijing Institute of Technology
Email: correspondent_dong@163.com

Abstract- Second-order generalized integrator (SOGI) based phase-locked loops (PLLs) are widely used for grid synchronization in single-phase grid-connected power converters. Previously, the estimated frequency of the PLL stage is fed back to the front-end SOGI block to make the conventional SOGI-PLL frequency-adaptive, which increases the implementation complexity, and makes the tuning sensitive, thus reducing stability margins. Alternatively, a frequency-fixed SOGI based PLL (briefly called FFSOGI-PLL) is proposed to ensure stability and simple implementation in this letter. It is commonly known that the in-phase and quadrature-phase signals generated by the frequency-fixed SOGI are of different amplitudes in the presence of frequency drifts, which causes second harmonic ripples in the estimated parameters of the PLL loop. To deal with this issue, a simple yet effective method is developed in FFSOGI-PLL. The standard SOGI-PLL is firstly introduced, followed by the working principle and small-signal model of FFSOGI-PLL. The FFSOGI-PLL is then compared with the SOGI-PLL in terms of stability and transient performance. Finally, experimental results are presented to demonstrate the effectiveness of FFSOGI-PLL.

Keywords: Phase-locked loop (PLL), second-order generalized integrator (SOGI), frequency-fixed SOGI, second harmonic ripple.

I. INTRODUCTION

Single-phase inverters are widely used as grid side converters that convert the power from the dc-bus and properly inject this power to the grid, with which the injected current has to be synchronized. In addition, the integration of renewable energy sources into the power grid must follow modern grid codes [1] [2] [3], which requires an injection of high quality power in the normal operation mode. That is, the grid-tied inverter should inject synhcronized grid currents of high power quality, which requires a good grid sychronization algorithm.

The power-based PLL (pPLL) [4], the enhanced PLL (EPLL) [5], and the orthogonal signal generator (OSG) based PLL (OSG-PLL) which can be implemented by combining pPLL and different OSGs [6] [7] [8] [9] together, are among the most popular single-phase PLLs. Especially, OSG-PLLs have attracted lots of attention within the areas of power electronics and power systems. Among a large number of reported OSG-PLLs, SOGI-PLL has become the commonly used single-phase PLL because of its low computational burden and high filtering capability.

SOGI-PLL has a simple implementation. It consists of a basic SOGI block to generate two quadrature signals from the input voltage [9]. To implement the synchronization function, these quadrature signals are sent to an embedded synchronous reference frame based PLL (SRF-PLL) [10]. In addition, for ensuring accuracy in situations of frequency deviations, the estimated frequency of the SRF-PLL loop is fed back to the SOGI part to make SOGI-PLL frequency-adaptive [9], [11]. However, the involved frequency adaptation process increases the implementation complexity, and makes the tuning sensitive, thus reducing stability margins. Recently, to ensure stability and simple implementation, several PLLs with frequency-fixed SOGI have been proposed in the literature [12] [13] [14]. However, they still suffer from some drawbacks and should be further improved. The PLL presented in [12] is computationally intensive, and sensitive to high-frequency noise because of the employed differentiation operator. It is well known that input frequency deviations in SOGI-PLLs with

frequency-fixed SOGI cause second harmonic ripples in the estimated parameters [9]. Hence, a new design rule to reduce such second harmonic ripples is presented in [13], [14]. It, however, cannot fully eliminate the second harmonic ripples and, therefore, cannot ensure zero steady-state error under varying frequency conditions.

In this letter, a new frequency-fixed SOGI based PLL (FFSOGI-PLL) is proposed to ensure stability and simple implementation. Considering possible frequency deviations, a simple yet effective method is applied to the generated quadrature signals of the frequency-fixed SOGI. As a result, the introduced FFSOGI-PLL can provide accurate synchronization performance even in the presence of frequency drifts. Moreover, FFSOGI-PLL contains no interdependent loops, thus offering enhanced stability and easy tuning process. The operational principle as well as the small-signal model of FFSOGI-PLL is presented in detail, together with experimental results for verifying its performance.

II. OVERVIEW OF THE SOGI-PLL

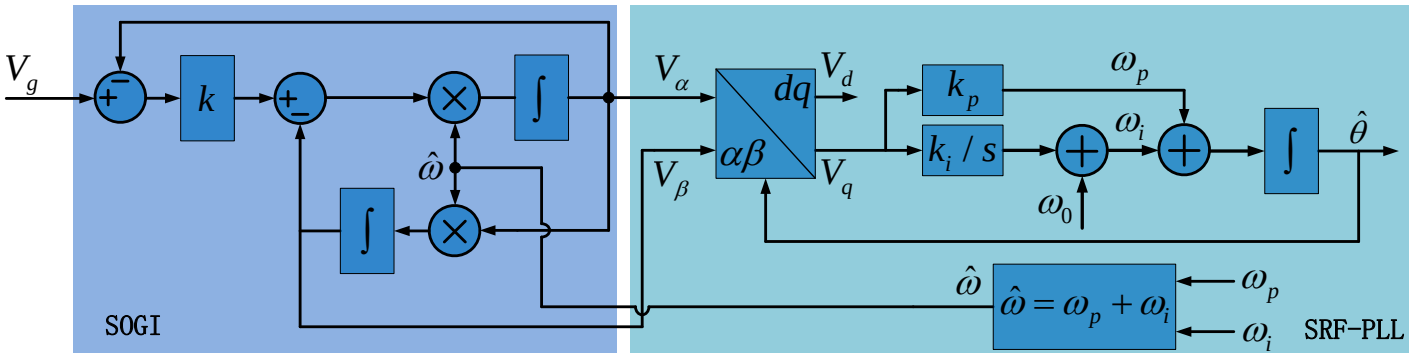

Fig. 1. The block diagram of the typical SOGI-PLL.

In this section, a brief overview of the typical SOGI-PLL is presented, followed by its small-signal model. The structure of the standard SOGI-PLL [9] is depicted in Fig. 1, where V_g represents the sampled grid voltage, ω_0 is the nominal grid frequency which is $2\pi 50$ rad/s in this work, and $\hat{\omega}$ and $\hat{\theta}$ are the estimated frequency and phase angle, respectively. Note that the estimated frequency is fed back to the SOGI block to make it frequency-adaptive. The park transformation ($\alpha\beta \rightarrow dq$) is defined as follows:

$$\begin{bmatrix} V_d \\ V_q \end{bmatrix} = \begin{bmatrix} \sin(\hat{\theta}) & -\cos(\hat{\theta}) \\ \cos(\hat{\theta}) & \sin(\hat{\theta}) \end{bmatrix} \begin{bmatrix} V_\alpha \\ V_\beta \end{bmatrix} \tag{1}$$

From Fig. 1, the characteristic transfer functions of the SOGI block can be derived as [15]

$$\begin{aligned} G_\alpha(s) &= \frac{V_\alpha(s)}{V_g(s)} = \frac{k\hat{\omega}s}{s^2 + k\hat{\omega}s + \hat{\omega}^2} \\ G_\beta(s) &= \frac{V_\beta(s)}{V_g(s)} = \frac{k\hat{\omega}^2}{s^2 + k\hat{\omega}s + \hat{\omega}^2} \end{aligned} \tag{2}$$

where k is the gain factor of SOGI. Assume the grid voltage to be $V_g = V_p \sin(\omega t) = V_p \sin(\theta)$, where V_p is the voltage amplitude, and ω and θ are the frequency and phase angle, respectively. For the purpose of simplicity, the voltage amplitude is assumed to be unity in the following discussions ($V_p = 1$). After some mathematical manipulations, the output signals of the SOGI block with $k < 2$ can be obtained as

$$\begin{aligned} V_\alpha(t) &= \frac{k\hat{\omega}\omega}{\sqrt{k^2\hat{\omega}^2\omega^2 + (\hat{\omega}^2 - \omega^2)^2}} \sin(\omega t - \delta) - \mathrm{A}\sin(\sqrt{1-(k/2)^2}\,\hat{\omega}t - \varphi_1)e^{-k\hat{\omega}t/2} \\ V_\beta(t) &= \frac{-k\hat{\omega}^2}{\sqrt{k^2\hat{\omega}^2\omega^2 + (\hat{\omega}^2 - \omega^2)^2}} \cos(\omega t - \delta) - \mathrm{B}\cos(\sqrt{1-(k/2)^2}\,\hat{\omega}t - \varphi_2)e^{-k\hat{\omega}t/2} \end{aligned} \tag{3}$$

where

$$\begin{aligned} \mathrm{A} &= \frac{k\omega\sqrt{4(4-k^2)(\omega^2-\hat{\omega}^2)^2\hat{\omega}^2 + [2k\hat{\omega}(\omega^2-\hat{\omega}^2) + 4k\hat{\omega}^3]^2}}{[k^2\hat{\omega}^4(4-k^2) + (k^2\hat{\omega}^2 - 2\hat{\omega}^2 + 2\omega^2)^2]\sqrt{1-(k/2)^2}} \\ \mathrm{B} &= \frac{2k\omega\hat{\omega}}{\sqrt{k^2\hat{\omega}^4(4-k^2) + (k^2\hat{\omega}^2 - 2\hat{\omega}^2 + 2\omega^2)^2}\sqrt{1-(k/2)^2}} \\ \sin(\delta) &= \frac{(\omega^2-\hat{\omega}^2)}{\sqrt{k^2\hat{\omega}^2\omega^2 + (\hat{\omega}^2-\omega^2)^2}},\quad \tan(\varphi_1) = \frac{\sqrt{(4-k^2)}(\omega^2-\hat{\omega}^2)}{k(\omega^2-\hat{\omega}^2) + 2k\hat{\omega}^2},\quad \tan(\varphi_2) = \frac{(k^2\hat{\omega}^2 - 2\hat{\omega}^2 + 2\omega^2)}{2k\hat{\omega}^2\sqrt{1-(k/2)^2}} \end{aligned} \tag{4}$$

Then, under the frequency-locked condition (i.e., $\hat{\omega} = \omega$), (3) can be rewritten as [15]

$$\begin{aligned} V_\alpha(t) &= \sin(\omega t) - \frac{1}{\sqrt{1-(k/2)^2}} \sin(\sqrt{1-(k/2)^2}\,\omega t)e^{-k\omega t/2} \\ V_\beta(t) &= -\cos(\omega t) - \frac{1}{\sqrt{1-(k/2)^2}} \cos(\sqrt{1-(k/2)^2}\,\omega t - \varphi_2)e^{-k\omega t/2},\quad \varphi_2 = \tan^{-1}\left(\frac{k}{\sqrt{4-k^2}}\right) \end{aligned} \tag{5}$$

As expected, in steady state, V_α and V_β are in phase and quadrature phase with the input voltage,

respectively. Applying the transformation matrix (1) to (5) yields V_d and V_q signals as expressed in

$$\begin{aligned} V_d(t) &= \cos(\theta-\hat{\theta}) - \{\sin(\sqrt{1-(k/2)^2}\,\omega t)\sin(\hat{\theta}) \\ &-\cos(\sqrt{1-(k/2)^2}\,\omega t-\varphi_2)\cos(\hat{\theta})\}\frac{1}{\sqrt{1-(k/2)^2}}e^{-k\omega t/2} \\ V_q(t) &= \sin(\theta-\hat{\theta}) - \{\sin(\sqrt{1-(k/2)^2}\,\omega t)\cos(\hat{\theta}) \\ &+\cos(\sqrt{1-(k/2)^2}\,\omega t-\varphi_2)\sin(\hat{\theta})\}\frac{1}{\sqrt{1-(k/2)^2}}e^{-k\omega t/2} \end{aligned} \tag{6}$$

It is worth noting that the second terms on the right-hand side of (6) decay to zero in steady state. Hence, under a small phase difference $(\theta-\hat{\theta})$, V_d yields an estimation of the voltage amplitude, and V_q gives the phase error information. In what follows, the small-signal model of SOGI-PLL is derived under assumptions: the estimated frequency is almost equal to the real one (i.e., $\hat{\omega}\cong\omega$), and the estimated phase angle $\hat{\theta}$ is approximately close to the real phase angle θ, thus, $\sin(\theta-\hat{\theta})\cong(\theta-\hat{\theta})$ and $\cos(\theta-\hat{\theta})\cong 1$.

It follows from (6) that the decaying terms decay to zero with a time constant of $2/(k\omega)$, and V_q converges to $\sin(\theta-\hat{\theta})\cong(\theta-\hat{\theta})$. Thus, for a step phase change, V_q can be approximated in s domain as [16]

$$V_q(s)\cong G_\tau(s)[\theta(s)-\hat{\theta}(s)],\quad G_\tau(s)=\frac{1}{\tau_p s+1},\ \tau_p=\frac{2}{k\omega} \tag{7}$$

Considering the possible voltage harmonics, V_q should be rewritten as follows [16]

$$V_q(s)\cong G_\tau(s)[\theta(s)-\hat{\theta}(s)]+D(s) \tag{8}$$

where, $D(s)$ represents the disturbances arising from voltage harmonics. The small-signal model of the typical SOGI-PLL can therefore be derived as shown in Fig. 2.

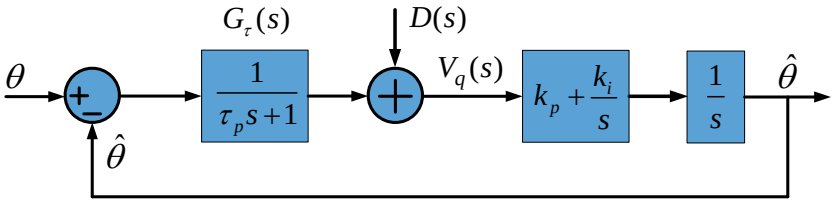

Fig. 2. The small-signal model of the typical SOGI-PLL.

III. DESCRIPTION OF THE PROPOSED FFSOGI-PLL

In this section, the FFSOGI-PLL as shown in Fig. 3 is developed to ensure stability and simple implementation. It can be observed that the SOGI block is tuned at the nominal frequency ω_0, thus decoupling the SOGI block and the SRF-PLL. Moreover, a simple yet effective method is applied to the generated signals V_α and V_β for ensuring accuracy in the presence of frequency drifts. In what follows, the operational principle and the small-signal model of FFSOGI-PLL are given.

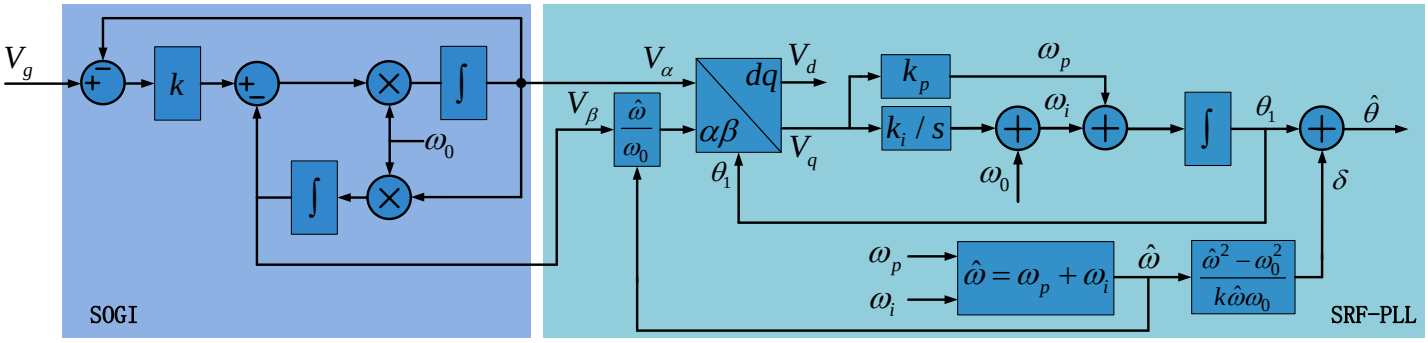

Fig. 3. The block diagram of the proposed FFSOGI-PLL.

A. Operational principle of the FFSOGI-PLL

Also from (3), V_α and V_β of the frequency-fixed SOGI in steady state can be achieved as

$$
\begin{aligned}
V_\alpha(t) &= \frac{k\omega_0\omega}{\sqrt{k^2\omega_0^2\omega^2 + (\omega_0^2 - \omega^2)^2}}\sin(\omega t - \delta) \\
V_\beta(t) &= \frac{-k\omega_0^2}{\sqrt{k^2\omega_0^2\omega^2 + (\omega_0^2 - \omega^2)^2}}\cos(\omega t - \delta) \\
\sin(\delta) &= \frac{\omega^2 - \omega_0^2}{\sqrt{k^2\omega_0^2\omega^2 + (\omega_0^2 - \omega^2)^2}}
\end{aligned}
\tag{9}
$$

It is obvious that V_α and V_β have different amplitudes if $\omega \neq \omega_0$, which causes second harmonic ripples in the estimated parameters of SOGI-PLLs based on frequency-fixed SOGI. A close observation of (9) reveals that the amplitude of V_α is ω/ω_0 times as large as that of V_β in steady state. In other words, V_α is orthogonal to $\frac{\omega}{\omega_0}V_\beta$ in steady state. Therefore, V_α and $\frac{\hat{\omega}}{\omega_0}V_\beta$ are used instead of V_α and V_β for ensuring

no second harmonic ripples in steady state as shown in Fig. 3. Note that, there exists a small phase difference δ between the real phase angle θ and that of V_α, which should be compensated. Given that $|\omega_0^2-\omega^2| \ll k\omega\omega_0$ (allowable frequency deviation range is generally small, such as 0.2 Hz in China), δ can be approximated as

$$\delta \cong \sin(\delta) \cong \frac{\hat{\omega}^2-\omega_0^2}{k\hat{\omega}\omega_0} \tag{10}$$

Thus, the estimated phase angle can be obtained as

$$\hat{\theta} = \theta_1 + \delta \tag{11}$$

Similarly, the amplitude of V_α is slightly different from the actual amplitude of the grid voltage, and the difference should be also compensated if a very accurate voltage amplitude estimation is required.

B. Small-signal model of the FFSOGI-PLL

To evaluate the small-signal stability of FFSOGI-PLL, its small-signal model is also derived under the same assumptions shown in the above section. Applying the transformation matrix (1) to (3) and (4) yields V_d and V_q signals in the FFSOGI-PLL as expressed in

$$\begin{aligned}
V_d(t) =& k_\theta \cos(\theta-\delta-\theta_1) + D_d(t) \\
&-[\mathrm{A}\sin(\sqrt{1-(k/2)^2}\,\omega_0 t-\varphi_1)\sin(\theta_1) - \mathrm{B}\cos(\sqrt{1-(k/2)^2}\,\omega_0 t-\varphi_2)\cos(\theta_1)]e^{-k\omega_0 t/2} \\
V_q(t) =& k_\theta \sin(\theta-\delta-\theta_1) + D_q(t) \\
&-[\mathrm{A}\sin(\sqrt{1-(k/2)^2}\,\omega_0 t-\varphi_1)\cos(\theta_1) + \mathrm{B}\cos(\sqrt{1-(k/2)^2}\,\omega_0 t-\varphi_2)\sin(\theta_1)]e^{-k\omega_0 t/2} \\
D_d(t) =& \frac{k\omega_0(\hat{\omega}-\omega)}{2\sqrt{k^2\omega_0^2\omega^2+(\omega_0^2-\omega^2)^2}}\cos(\theta-\delta+\theta_1),\ D_q(t) = \frac{k\omega_0(\omega-\hat{\omega})}{2\sqrt{k^2\omega_0^2\omega^2+(\omega_0^2-\omega^2)^2}}\sin(\theta-\delta+\theta_1) \\
k_\theta =& \frac{k\omega_0\omega}{\sqrt{k^2\omega_0^2\omega^2+(\omega_0^2-\omega^2)^2}} - \frac{k\omega_0(\omega-\hat{\omega})}{2\sqrt{k^2\omega_0^2\omega^2+(\omega_0^2-\omega^2)^2}}
\end{aligned} \tag{12}$$

in which, A, B, φ_1, and φ_2 are obtained by replacing $\hat{\omega}$ with the nominal frequency ω_0 in (4). Since the allowable frequency variation range in the normal operation mode is relatively small such as 0.2 Hz in China, $|\omega-\hat{\omega}| \ll 2\omega$ is satisfied so that

$$k_\theta \cong \frac{k\omega_0\omega}{\sqrt{k^2\omega_0^2\omega^2+(\omega_0^2-\omega^2)^2}} \cong 1 \tag{13}$$

As shown in (12), the decaying terms decay to zero with a time constant $\tau_p = 2/(k\omega_0)$, and V_q converges to $k_\theta \sin(\theta - \delta - \theta_1) \cong (\theta - \delta - \theta_1)$. D_d and D_q represent the additional oscillating components due to $\hat{\omega} \neq \omega$, and become zero under the frequency locked condition (i.e., $\hat{\omega} = \omega$). For a step phase change, the corresponding signal V_q can be approximately expressed in s domain as

$$\begin{aligned} &V_q(s) \cong k_\theta[\theta'(s) - \theta_1(s)] + D_q(s) \\ &D_q(s) = L[D_q(t)], \quad \theta'(s) = G_\tau(s)\theta(s), \; G_\tau(s) = \frac{1}{\tau_p s + 1}, \; \tau_p = \frac{2}{k\omega_0} \end{aligned} \tag{14}$$

where θ' is the real phase angle of V_α and L denotes the Laplace operator. Considering the possible voltage harmonics as well, V_q should be rewritten as follows:

$$V_q(s) \cong k_\theta[\theta'(s) - \theta_1(s)] + D'(s), \quad D'(s) = D(s) + D_q(s) \tag{15}$$

where $D(s)$ represents the disturbances arising from voltage harmonics. Thus, the small-signal model of the FFSOGI-PLL can be derived as shown in Fig. 4. Similarly, $D'(s)$ appears as a disturbance input to the PLL small-signal model. Due to the decoupled structure of the FFSOGI-PLL, the approximated block $G_\tau(s)$ for the SOGI block acts as a pre-filter, and has no influence on the system stability. In contrast, $G_\tau(s)$ is inside the closed feedback loop of the SOGI-PLL as shown in Fig. 2, and affects the system stability.

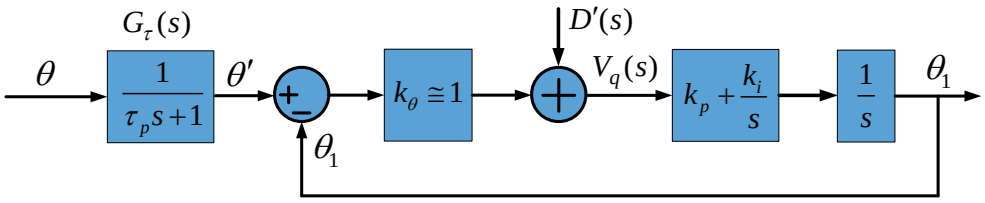

Fig. 4. The small-signal model of the proposed FFSOGI-PLL.

To evaluate the accuracy of the derived small-signal model of FFSOGI-PLL, the actual FFSOGI-PLL and its model are simulated, and their results under a phase angle jump and a frequency step change are obtained and compared to each other. The corresponding simulation results are depicted in Fig. 5. It is clear that the derived model can well predict the dynamic behavior of FFSOGI-PLL. A phase offset can be observed in the presence

of frequency drifts, which should be compensated by using (11) as shown in Fig. 3.

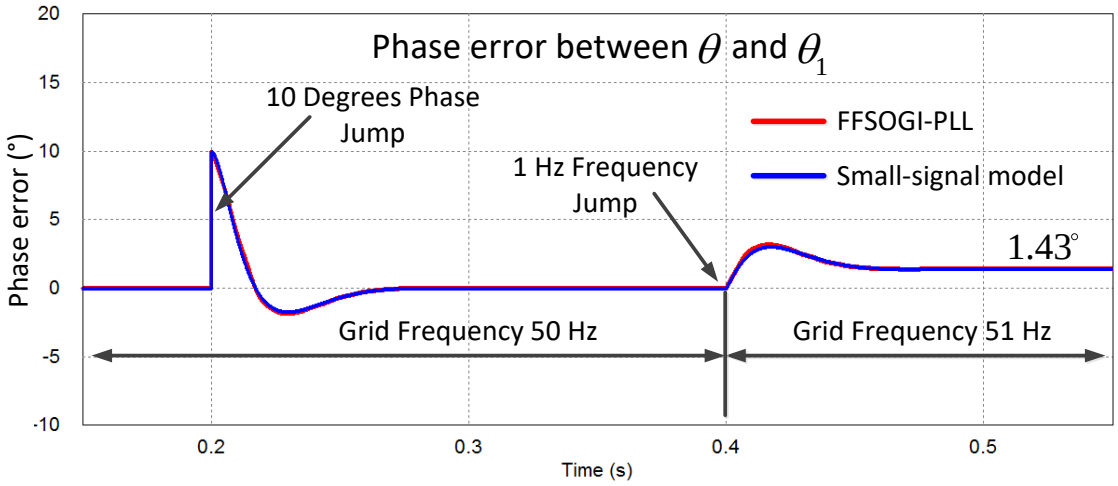

Fig. 5. Accuracy assessment of the FFSOGI-PLL small-signal model with $k_p = 137.5$, $k_i = 7878$, $k = 1.63$, $\omega_0 = 2\pi 50$ rad/s, and $T_s = 1e-4$ s.

IV. Comparison between SOGI-PLL and FFSOGI-PLL

In this section, the typical SOGI-PLL is compared with the proposed FFSOGI-PLL in terms of the system stability as well as the transient performance.

A. Small signal stability comparison

The open-loop and closed-loop transfer functions of the standard SOGI-PLL can be obtained from Fig. 2 as

$$G_{ol\_SOGI}(s) = \frac{k_p s + k_i}{s^2(\tau_p s + 1)}$$
$$G_{cl\_SOGI}(s) = \frac{\hat{\theta}(s)}{\theta(s)} = \frac{k_p s + k_i}{\tau_p s^3 + s^2 + k_p s + k_i} \tag{16}$$

According to the Routh–Hurwitz stability criterion, the corresponding stability condition is

$$k_p > \tau_p k_i \tag{17}$$

while the open-loop and closed-loop transfer functions of the FFSOGI-PLL can be derived from Fig. 4 as

$$G_{ol\_FFSOGI}(s) = \frac{k_\theta (k_p s + k_i)}{s^2}$$
$$G_{cl\_FFSOGI}(s) = \frac{\theta_1(s)}{\theta(s)} = G_\tau(s)\frac{k_\theta (k_p s + k_i)}{s^2 + k_\theta k_p s + k_\theta k_i} = G_\tau(s)\frac{2\zeta\omega_n s + \omega_n^2}{s^2 + 2\zeta\omega_n s + \omega_n^2} \tag{18}$$

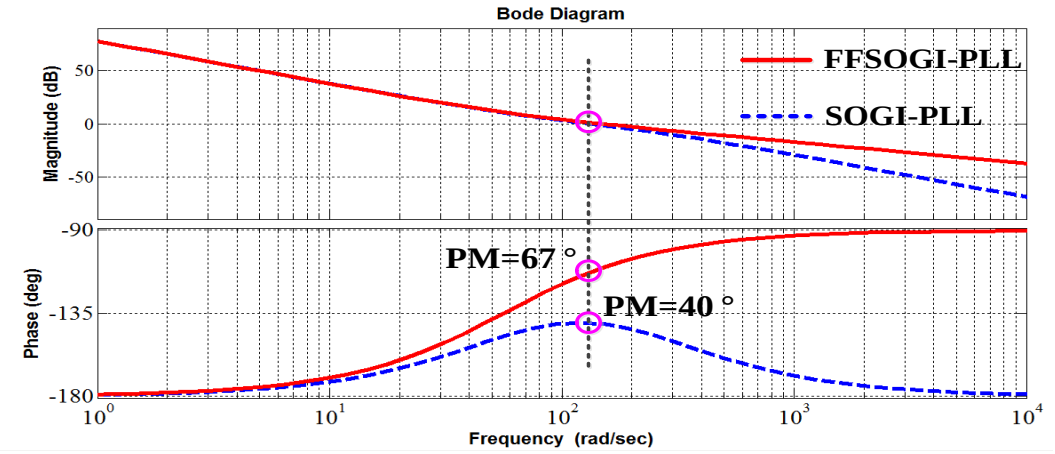

Fig. 6. Bode plots of the SOGI-PLL and FFSOGI-PLL with $k_p = 137.5$ and $k_i = 7878$.

where ω_n and ζ represent the natural frequency and damping factor, respectively. For such a third-order system, it is always stable for any given positive k_p and k_i, which implies that the presented FFSOGI-PLL is superior to the typical SOGI-PLL in terms of system stability. The gain factor k is designed as 1.63 for the minimum settling time of the SOGI part in both the SOGI-PLL and FFSOGI-PLL [14]. The tuning of k_p and k_i involves tradeoffs among the speed of response, overshoot, stability margin, and filtering capability, which has been well discussed in many publications [16], [17]. Here, $k_p = 137.5$ and $k_i = 7878$ are selected for the SOGI-PLL according to [16]. For the comparison purpose, the same control parameters are used in the FFSOGI-PLL. The bode plots of the $G_{ol\_SOGI}(s)$ and $G_{ol\_FFSOGI}(s)$ are plotted in Fig. 6. It is clear that the FFSOGI-PLL has nearly the same performance as the SOGI-PLL in the low-frequency range. However, the FFSOGI-PLL provides a higher phase margin, hence, a more stable operation.

B. Transient performance comparison

The PLL technique generally suffers from large frequency transient during phase jumps [18]. This is because the frequency and phase angle are estimated within a single loop as shown in both Fig. 1 and Fig. 3. In SOGI-PLL, the propagation of the large frequency transient to the SOGI block makes the produced signals V_α and V_β oscillatory, which is reflected back on the SRF-PLL stage. Consequently, the SOGI-PLL becomes oscillatory, and may even become unstable during large phase jumps. To avoid this issue, the PI controller with

smaller k_p and k_i is often designed at the expense of slower dynamic response in SOGI-PLL. In contrast, the front-end SOGI block is tuned at the nominal frequency in FFSOGI-PLL, which, hence, can avoid the afore-mentioned stability problem. As a result, the proposed FFSOGI-PLL provides a possibility to select larger k_p and k_i than the typical SOGI-PLL for a faster dynamic response. For example, $\zeta = 0.707$ and $\omega_n = 2\pi 32$ rad/s can be chosen in the FFSOGI-PLL, which results in $k_p = 284$ and $k_i = 40385$.

As shown in both Fig. 1 and Fig. 3, the sum of the integral part ω_i and the proportional term ω_p is used as the frequency estimation $\hat{\omega}$. However, the proportional term ω_p is k_p times as large as the input error signal without any filtering capability, so large ω_p happens in the presence of large phase jumps/voltage drops, which not only increases the transient frequency errors, but also has great impact on the system stability of SOGI-PLL as mentioned above. To attenuate the negative effects of the proportional term ω_p on frequency estimation as well as stability in the SOGI-PLL, the integral term ω_i instead of the sum $(\omega_i + \omega_p)$ can be used as the frequency estimation $\hat{\omega}$ [19]. In this way, more filtered frequency estimation and enhanced stability can be achieved in SOGI-PLL. It is worth noting that the same modification also can be applied to the FFSOGI-PLL for achieving more filtered frequency estimation. Due to space limitation, the simulation results are neglected here, and the stability analysis will be carried in the future work.

Also note that SOGI has good rejection capability on high-order harmonics and high-frequency noise so that both the SOGI-PLL and FFSOGI-PLL can perform well in most cases. Nevertheless, these two PLLs cannot effectively address dc offset and low-order harmonics, which have been well studied in lots of reported work [20] [21] [22] [23] and, therefore, will not be further discussed for simplicity in this letter.

V. Experimental Results

In this section, the performance of the proposed FFSOGI-PLL is evaluated under several grid disturbances including 1 Hz frequency jump, 30% voltage drop, and 20 degrees phase jump. In obtaining all results, the

sampling frequency is fixed at 10 kHz frequency. To provide a base for comparison, the typical SOGI-PLL is also implemented, and its results are compared with those of FFSOGI-PLL. The considered parameters used in the first three test cases are shown in Table I.

Table I. Control Parameters used in the first three test cases

	FFSOGI-PLL				SOGI-PLL			
	k_p	k_i	ω_n (rad/s)	ζ	k_p	k_i	ω_n (rad/s)	Z
Case I	137.5	7878	$2\pi 14.1$	0.78	137.5	7878	$2\pi 21.88$	0.7
Case II	284	40385	$2\pi 32$	0.707	137.5	7878	$2\pi 21.88$	0.7
Case III	284	40385	$2\pi 32$	0.707	284	40385	$2\pi 45.2$	0.5

Fig. 7 shows the experimental results of the test cases I. It can be observed from Fig. 7 that, with the same control parameters, the FFSOGI-PLL has nearly the same dynamic performance, but smaller overshoots and/or undershoots in comparison to the SOGI-PLL. In addition, Fig. 8 and Fig. 9 depict the experimental results of the test cases II and III, respectively. It is worth noting that, the FFSOGI-PLL with $k_p = 284$ and $k_i = 40385$ provides faster transient responses than the SOGI-PLL with $k_p = 137.5$ and $k_i = 7878$, while the SOGI-PLL with $k_p = 284$ and $k_i = 40385$ becomes oscillatory and requires much longer time to settle to a new steady state. It implies that the FFSOGI-PLL can achieve a faster response, while not affecting the system stability.

As mentioned above, to obtain a more filtered frequency estimation, the frequency estimation can be taken only from the integral term ($\hat{\omega} = \omega_p$) in both the SOGI-PLL and FFSOGI-PLL, and the modified SOGI-PLL and FFSOGI-PLL are termed as MSOGI-PLL and MFFSOGI-PLL, respectively. Due to space limitation, these four PLLs are only compared to each other under 20 degrees phase jump. Here, two additional test cases are considered, $k_p = 137.5$ and $k_i = 7878$ are adopted for these four PLLs in the test case IV, while $k_p = 284$ and $k_i = 40385$ are used for them in the test case V. The corresponding results are shown in Fig. 10 and Fig.

11, respectively. It can be observed that both MSOGI-PLL and MFFSOGI-PLL exhibit smaller transient frequency errors than SOGI-PLL and FFSOGI-PLL, respectively. Besides, MSOGI-PLL provides better stability margin than SOGI-PLL as shown in Fig. 11(a). From Fig. 10(c) and Fig. 11(c), the experimental results show that MFFSOGI-PLL performs better than MSOGI-PLL in terms of dynamic performance and stability. Therefore it is worth doing further research on the MFFSOGI-PLL in terms of stability analysis which will be one of the focuses of our future work.

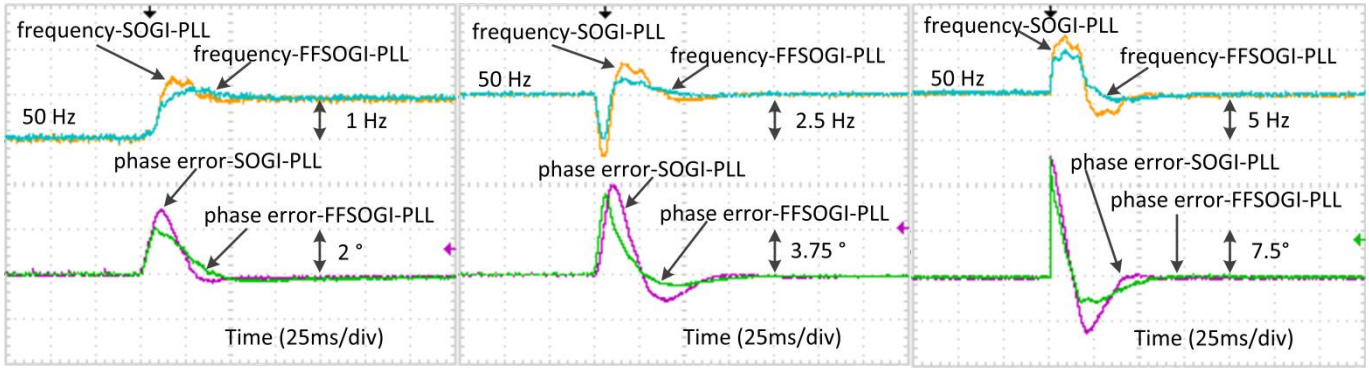

(a) 1 Hz Frequency jump. (b) 30% Voltage drop. (c) 20 Degrees phase jump.

Fig. 7. Experimental results of the test case I.

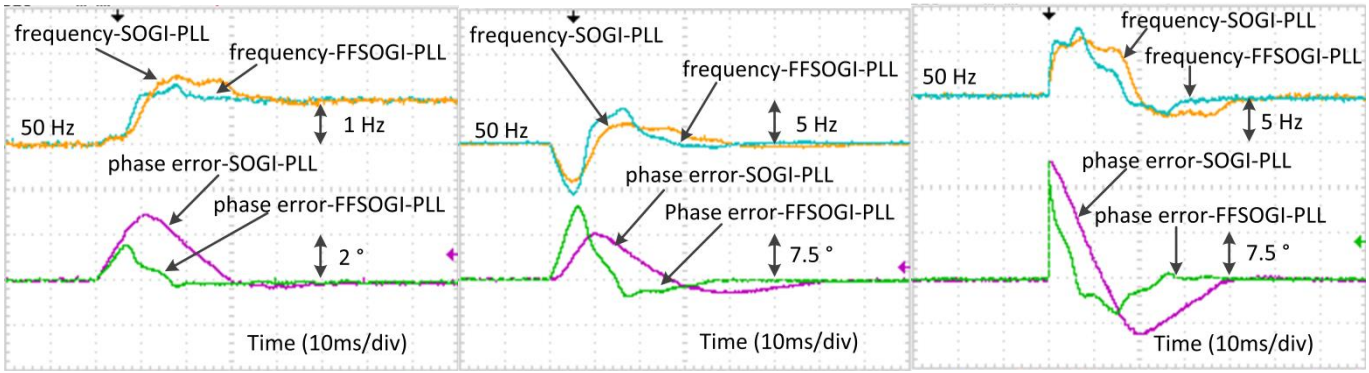

(a) 1 Hz Frequency jump. (b) 30% Voltage drop. (c) 20 Degrees phase jump.

Fig. 8. Experimental results of the test case II.

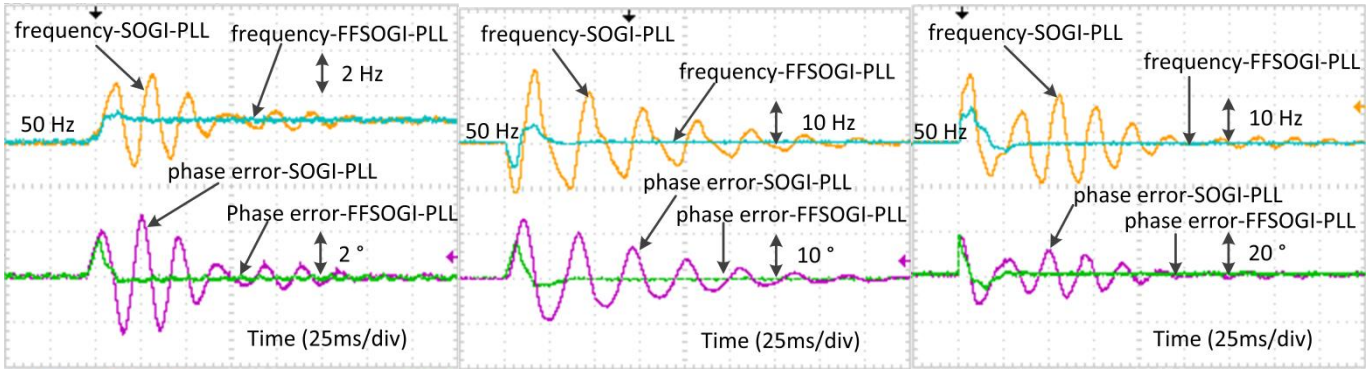

(a) 1 Hz Frequency jump. (b) 30% Voltage drop. (c) 20 Degrees phase jump.

Fig. 9. Experimental results of the test case III.

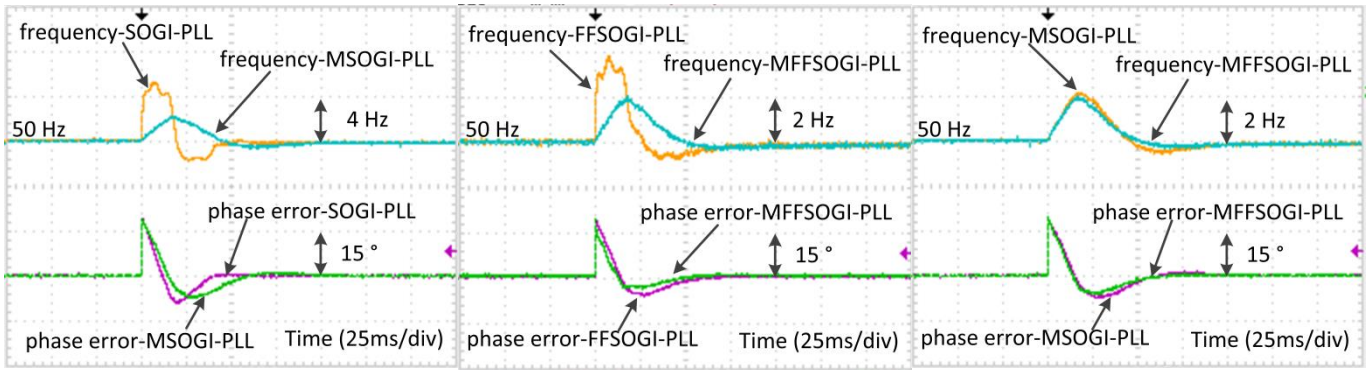

(a) SOGI-PLL and MSOGI-PLL. (b) FFSOGI-PLL and MFFSOGI-PLL. (c) MSOGI-PLL and MFFSOGI-PLL.

Fig. 10. Experimental results of the test case IV.

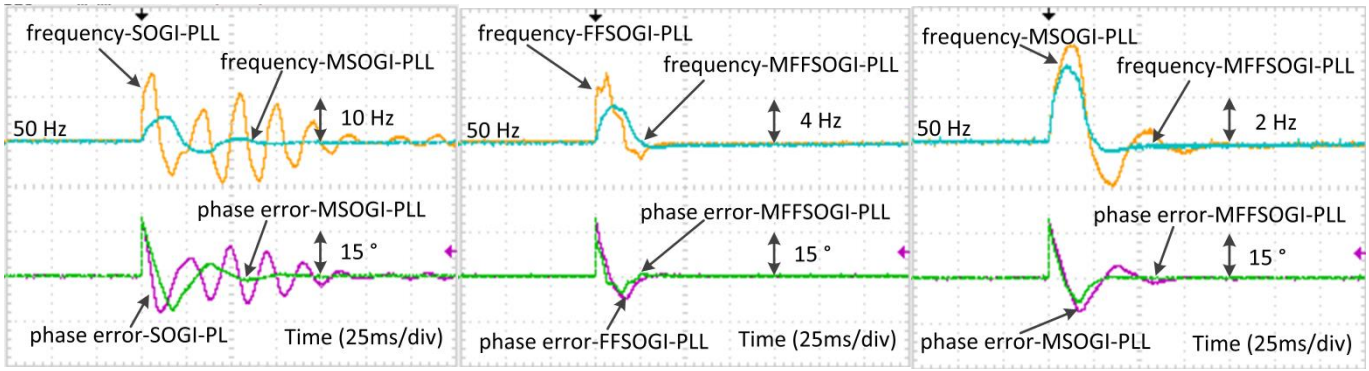

(a) SOGI-PLL and MSOGI-PLL. (b) FFSOGI-PLL and MFFSOGI-PLL. (c) MSOGI-PLL and MFFSOGI-PLL.

Fig. 11. Experimental results of the test case V.

VI. CONLUSIONS

In this letter, the FFSOGI-PLL based on a frequency-fixed SOGI is proposed to ensure stability and simple implementation. To ensure accuracy under varying frequency conditions, a simple yet effective method is then

applied to the generated quadrature signals of the frequency-fixed SOGI. The standard SOGI-PLL is firstly studied, followed by the working principle and small-signal model of the FFSOGI-PLL. Subsequently, the FFSOGI-PLL is compared with the SOGI-PLL in terms of the system stability and transient performance. In addition, the possibility to further improve the SOGI-PLL and FFSOGI-PLL by taking the frequency estimation from the integral channel of the PI is explored. Finally, experimental results are presented to demonstrate the effectiveness of the FFSOGI-PLL.

REFERENCES

[1] IEEE Standard for Interconnecting Distributed Resources with Electric Power Systems, IEEE Std. 1547-2003, pp. 1–27, 2003.

[2] B.-I. Craciun, T. Kerekes, D. Sera, and R. Teodorescu, "Overview of recent grid codes for PV power integration," in Proc. OPTIM, pp. 959–965, 2012.

[3] R. Teodorescu, M. Liserre, and P. Rodriguez, "Grid Converters for Photovoltaic and Wind Power Systems," New York, NY, USA: Wiley, 2011.

[4] R. M. Santos Filho, P. F. Seixas, P. C. Cortizo, L. A. B. Torres, and A. F. Souza, "Comparison of three single-phase PLL algorithms for UPS applications," IEEE Trans. Ind. Electron., vol. 55, no. 8, pp. 2923-2932, August 2008.

[5] M. Karimi-Ghartemani, and M. R. Iravani, "A method for synchronization of power electronic converters in polluted and variable-frequency environments," IEEE Trans. Power Syst., vol. 19, no. 3, pp. 1263-1270, August 2004.

[6] R. Zhang, M. Cardinal, P. Szczesny, and M. Dame, "A grid simulator with control of single-phase power converters in D–Q rotating frame," in Proc. IEEE Power Electron. Spec. Conf., pp. 1431-1436, 2002.

[7] R. Y. Kim, S. Y. Choi, and I. Y. Suh, "Instantaneous control of average power for grid tie inverter using single phase D–Q rotating frame with all pass filter," in Proc. IEEE Ind. Electron. Conf., Busan, Korea, pp. 274-279, 2004.

[8] M. Saitou, and T. Shimizu, "Generalized theory of instantaneous active and reactive powers in single-phase circuits based on Hilbert transform," in Proc. 33rd Annu. IEEE PESC, pp. 1419-1424, 2002.

[9] M. Ciobotaru, R. Teodorescu, and F. Blaabjerg, “A new single-phase PLL structure based on second order generalized integrator,” in Proc. 37th IEEE PESC, pp. 1511-1516, 2006.

[10] A. Kulkarni and V. John, “A novel design method for SOGI-PLL for minimum settling time and low unit vector distortion,” in 39th Annual Conference of the IEEE Industrial Electronics Society-IECON 2013, pp. 274–279, Nov 2013.

[11] Y. Yang and F. Blaabjerg, “Synchronization in single-phase grid-connected photovoltaic systems under grid faults,” in 3rd IEEE International Symposium on Power Electronics for Distributed Generation Systems (PEDG), pp. 476–482, June 2012.

[12]M. Reza, M. Ciobotaru, and V. G. Agelidis, “Estimation of single-phase grid voltage fundamental parameters using fixed frequency tuned second-order generalized integrator based technique,” In Power Electronics for Distributed Generation Systems (PEDG), IEEE, pp. 1-8, July 2013.

[13] A. Kulkarni and V. John, “A novel design method for SOGI-PLL for minimum settling time and low unit vector distortion,” In Industrial Electronics Society, IECON 2013-39th Annual Conference of the IEEE, pp. 274-279, November 2013.

[14] A. Kulkarni and V. John, “Design of a Fast Response Time Single-Phase PLL with DC Offset Rejection Capability,” SAE Technical Paper, 2015.

[15] Teodorescu, R., Liserre, M. and Rodriguez, P., Grid Converters for Photovoltaic and Wind Power Systems. Hoboken, NJ: IEEE-Wiley, 2011.

[16]S. Golestan, M. Monfared, F. D. Freijedo, and J. M. Guerrero, “Dynamics assessment of advanced single-phase PLL structures,” IEEE Trans. Ind. Electron., vol. 60, no. 6, pp. 2167-2177, June 2013.

[17] F. D. Freijedo, J.Doval-Gandoy, O. Lopez, andE.Acha, “Tuning of phase-locked loops for power converters under distorted utility conditions,” IEEE Trans. Ind. Appl., vol. 45, no. 6, pp. 2039–2047, Nov. 2009.

[18] M. K. Ghartemani, S. A. Khajehoddin, P. K. Jain, and A. Bakhshai, “Problems of startup and phase jumps in PLL systems,” IEEE Trans. Power Electron., vol. 27, no. 4, pp. 1830–1838, Apr. 2012.

[19] S. Golestan, J. M. Guerrero, A. Vidal, A. G. Yepes, J. Doval-Gandoy, and F. D. Freijedo, "Small-Signal Modeling, Stability Analysis and Design Optimization of Single-Phase Delay-Based PLLs," IEEE Trans. Power Electron., vol. 31, no. 5, pp. 3517-3527, May 2016.

[20] K.-J. Lee, J.-P. Lee, D. Shin, D.-W. Yoo, and H.-J. Kim, “A novel grid synchronization PLL method based on adaptive low-pass notch filter for grid-connected PCS,” IEEE Trans. Ind. Electron., vol. 61, no. 1, pp. 292-301, Jan. 2014.

[21] S. Golestan, M. Ramezani, J. M. Guerrero, et al., “Moving Average Filter Based Phase-Locked Loops: Performance

Analysis and Design Guidelines," IEEE Trans. Power Electron., vol. 29, no. 6, pp. 2750-2763, June 2014.

[22] F. Wu, D. Sun, et al., "Influence of Plugging DC Offset Estimation Integrator in Single-Phase EPLL and Alternative Scheme to Eliminate Effect of Input DC Offset and Harmonics," IEEE Trans. Ind. Electron., vol. 62, no. 8, pp. 4823-4831, Aug. 2015.

[23] L. Hadjidemetriou, E. Kyriakides, Y. Yang and F. Blaabjerg, "A synchronization method for single-phase grid-tied inverters," IEEE Trans. Power Electron., vol. 31, no. 3, pp. 2139-2149, March 2016.